Polarization mapping of laser-induced monospectral fields of optically anisotropic fluorophores in forensic diagnostics of the age of the formation of damage to human organs

Litvinenko[1] A., Tryfonyuk[2] L., Pavlyukovich[1] O., Pavlyukovich[1] N., Stashkevich[3] A.T., Olar[4] O., Kurek[4] O.I., Tkachuk[4] V.I.
[1]Bukovinian State Medical University, Chernivtsi, Ukraine
[2]Rivne State Medical Hospital, Rivne, Ukraine
[3]The Institute of Traumatology and Orthopedics by NAMS of Ukraine, Kyiv, Ukraine
[4] Chernivtsi National University, Chernivtsi, Ukraine
cablaze9@gmail.com

ABSTRACT

The paper presents the results of experimental testing of methods for azimuthal-invariant polarization mapping of laser-induced microscopic images of fluorophores in histological sections of the liver of deceased; time monitoring of changes in the magnitude of statistical moments of the 1st - 4th orders characterizing the distributions of the azimuth and ellipticity of polarization of microscopic images of histological sections of the liver with different age of damage; determination of the diagnostic efficiency (time interval and accuracy) of establishing the age of damage to human internal organs by digital histological methods of mapping maps of azimuth and ellipticity of polarization of microscopic images of samples of histological sections of the brain, liver and kidney, as well as myocardium and lung tissue.

Keywords: polarization, azimuth, ellipticity, microscopic image, statistical moments of the 1st - 4th orders, histological sections, biological tissues, damages

1. INTRODUCTION

The methodology and technique of polarization mapping of microscopic images of biological preparations are presented in detail and comprehensively in numerous publications of the scientific schools [1-8].

The obtained results of polarization mapping revealed information (diagnostic) relationships between:

- maps of polarization azimuth and concentration of optically active molecular compounds (fluorophores) of biological tissues and fluids of human organs;
- maps of ellipticity of polarization and the degree of ordering (crystallization) of fibrillar networks of biological preparations.

However, at present, these digital methods of polarizing microscopy are practically absent in histological studies for determining the age of damage to human internal organs..

The aim of the study is to develop a set of objective forensic criteria for expanding the functionality and improving the accuracy of establishing the age of damage to human internal organs according to the data of a multiparametric digital histological study of liver tissue through the integrated use of polarization mapping of the polycrystalline structure of fluorophores of prototypes based on a statistical analysis of the temporal dynamics of their change [9-15].

2. MATERIALS AND METHODS

The following groups were formed (control group with those who died from coronary artery disease and experienced with different age of damage) of experimental samples of histological sections of internal organs (brain, liver, kidney, as well as myocardium and lung tissue) of a person.

Fifteenth International Conference on Correlation Optics, edited by Oleg V. Angelsky, Proc. of SPIE Vol. 12126, 1212622
© 2021 SPIE · 0277-786X · doi: 10.1117/12.2616662

Internal organ Brain, Liver, Kidney, Myocardium, Lung tissue	Groups								
	Control	Experienced with different age of damage, hours							
	Deceased from CAD(21)	1	6	12	18	24	48	72	96	120
		21	21	21	21	21	21	21	21	21

Within each of the groups:

- obtained maps of azimuth and polarization ellipticity of microscopic images;
- the statistical moments of the 1st - 4th orders were calculated, characterizing the distributions of the azimuth and ellipticity of the polarization;
- was determined within the control and the set of research groups, the average value and the error of the magnitude of each of the statistical moments of the 1st - 4th orders;
- the duration of the damage and its accuracy were calculated algorithmically.

3. DIFFERENTIAL DIAGNOSIS OF THE AGE OF THE FORMATION OF INJURIES OF INTERNAL ORGANS OF A PERSON BY MAPPING THE AZIMUTH OF POLARIZATION MAPS

Fig. 1 illustrates the data of digital polarization histology of the azimuth of polarization of microscopic images of histological sections of the liver from a research ((1), (4)) and two control ((2), (3), (5), (6)) groups of samples.

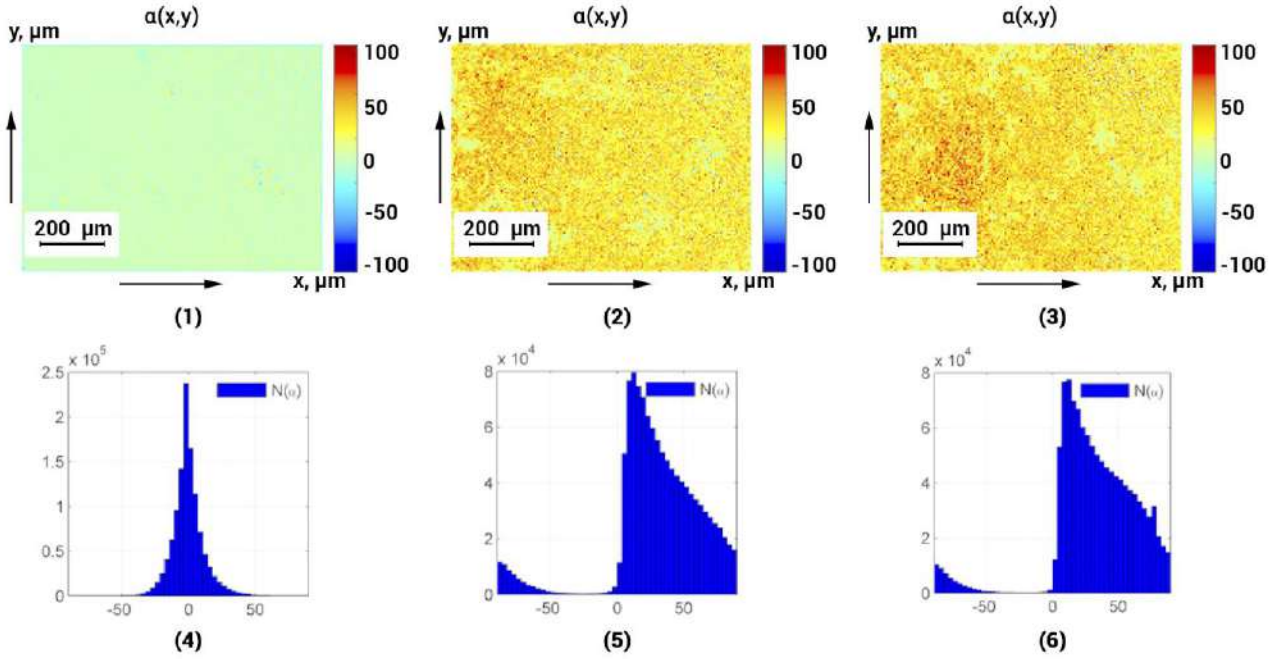

Fig. 1. Maps ((1), (2), (3)) and histograms ((4), (5), (6)) of distributions of the polarization azimuth of microscopic images (x4) of histological sections of the liver of deceased.

Table 1 Time dynamics of changes in statistical moments of the 1st - 4th orders characterizing the distribution of AP

T, hours	**1**	**4**	**6**	**12**	**18**
SM_1	$0{,}33 \pm 0{,}017$	$0{,}29 \pm 0{,}016$	$0{,}31 \pm 0{,}017$	$0{,}28 \pm 0{,}015$	$0{,}26 \pm 0{,}014$
p	$p \succ 0{,}05$				
SM_2	$0{,}24 \pm 0{,}014$	$0{,}21 \pm 0{,}012$	$0{,}19 \pm 0{,}011$	$0{,}21 \pm 0{,}012$	$0{,}18 \pm 0{,}0105$
p	$p \succ 0{,}05$				
SM_3	$0{,}76 \pm 0{,}036$	$0{,}92 \pm 0{,}043$	$1{,}11 \pm 0{,}052$	$1{,}42 \pm 0{,}068$	$1{,}32 \pm 0{,}064$
p	$p \prec 0{,}05$				$p \succ 0{,}05$
SM_4	$0{,}54 \pm 0{,}026$	$0{,}65 \pm 0{,}31$	$0{,}78 \pm 0{,}034$	$1{,}02 \pm 0{,}042$	$0{,}96 \pm 0{,}045$
p	$p \prec 0{,}05$				$p \succ 0{,}05$
T, hours	**24**	**30**	**36**	**42**	**48**
SM_1	$0.23 \pm 0{,}013$	$0{,}24 \pm 0{,}014$	$0{,}27 \pm 0{,}015$	$0{,}22 \pm 0{,}012$	$0{,}21 \pm 0{,}012$
p	$p \succ 0{,}05$				
SM_2	$0{,}17 \pm 0{,}009$	$0{,}15 \pm 0{,}008$	$0{,}17 \pm 0{,}009$	$0{,}18 \pm 0{,}0105$	$0{,}15 \pm 0{,}008$
p	$p \succ 0{,}05$				
SM_3	$1{,}34 \pm 0{,}071$	$1{,}38 \pm 0{,}069$	$1{,}36 \pm 0{,}073$	$1{,}39 \pm 0{,}075$	$1{,}38 \pm 0{,}074$
p	$p \succ 0{,}05$				
SM_4	$1{,}02 \pm 0{,}054$	$1{,}06 \pm 0{,}056$	$1{,}13 \pm 0{,}063$	$1{,}11 \pm 0{,}065$	$1{,}14 \pm 0{,}066$
p	$p \succ 0{,}05$				

The polarization maps (Fig. 1, fragments (1) - (3) of microscopic images of histological sections of the intact and damaged liver are coordinate-inhomogeneous (Fig. 1, fragments (4) - (6)).

It has been experimentally established that the spread in the azimuth value decreases with an increase in the age of damage - 6 hours. (Fragment (5)) and 18 hours (Fragment (6)), respectively (Table 1).

The results of the statistical analysis of the data presented in Table 1 revealed the diagnostic capabilities of a digital polarization histological study of the age of liver damage in the linear ($p \prec 0{,}05$) range of changes in the value of skewness (dynamic range 0.66) and kurtosis (dynamic range 0.48), characterizing the distributions of the polarization azimuth of microscopic images at a time interval of up to 12 hours

A series of fragments in Fig. 2 shows large-scale (40x) azimuth maps of images of histological sections of the liver.

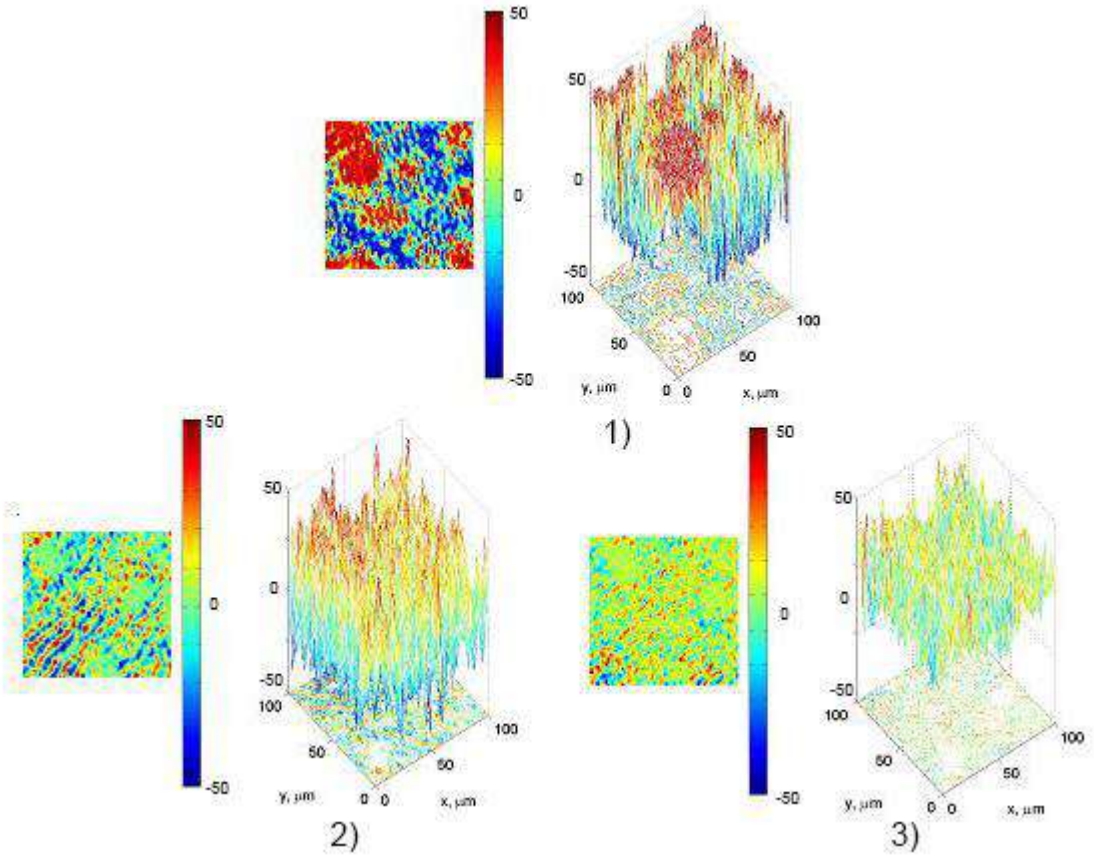

Fig. 2. Maps (fragments (1), (2), (3)) and coordinate distributions (fragments (4), (5), (6)) of the azimuth of polarization of microscopic images (x40) of histological sections of the liver of deceased from the control group (fragments (1), (4)), research groups with different duration of damage (6 hours - fragments (2), (5)) and (18 hours - fragments (3), (6)).

Large-scale maps of polarization azimuth of the liver are characterized by a large range (Fig. 3, fragments (2), (4), (6)) and significant coordinate inhomogeneity (Fig. 3, fragments (1), (3), (5)) of fluctuations of azimuth values, - table 2.

The following diagnostic statistically significant () indicators have been established:

- dispersion of the scatter of the azimuth of polarization of microscopic images (40x) of histological sections of the liver, the value of which varies linearly over a time interval of up to 6 hours (Dynamic range 0.09);
- skewness (dynamic range 1.25) and kurtosis (dynamic range 1.23) are characterized by a large linear range (up to 18 hours) and dynamics (up to 3 times) of change (compared to the data in Table 3.3) of its own value.

Table 2 Time dynamics of changes in the statistical moments of the 1st - 4th orders, characterizing the distribution of the AP value of microscopic images (40x) of histological sections of the liver

T, hours	**2**	**4**	**6**	**12**	**18**
SM_1	$0{,}26 \pm 0{,}015$	$0{,}23 \pm 0{,}014$	$0{,}21 \pm 0{,}012$	$0{,}23 \pm 0{,}014$	$0{,}22 \pm 0{,}012$
p	$p \succ 0{,}05$				
SM_2	$0{,}18 \pm 0{,}001$	$0{,}17 \pm 0{,}009$	$0{,}19 \pm 0{,}011$	$0{,}17 \pm 0{,}009$	$0{,}18 \pm 0{,}0105$
p		$p \prec 0{,}05$	$p \succ 0{,}05$		

SM_3	$0{,}83 \pm 0{,}036$	$1{,}04 \pm 0{,}046$	$1{,}27 \pm 0{,}052$	$1{,}64 \pm 0{,}078$	$2{,}08 \pm 0{,}094$
p	$p \prec 0{,}05$				
SM_4	$0{,}63 \pm 0{,}026$	$0{,}81 \pm 0{,}35$	$0{,}98 \pm 0{,}044$	$1{,}42 \pm 0{,}067$	$1{,}79 \pm 0{,}078$
p	$p \prec 0{,}05$				
T, hours	**24**	**30**	**36**	**42**	**48**
SM_1	$0.21 \pm 0{,}013$	$0{,}19 \pm 0{,}012$	$0{,}17 \pm 0{,}011$	$0{,}21 \pm 0{,}012$	$0{,}18 \pm 0{,}011$
p	$p \succ 0{,}05$				
SM_2	$0{,}16 \pm 0{,}009$	$0{,}19 \pm 0{,}011$	$0{,}15 \pm 0{,}009$	$0{,}13 \pm 0{,}008$	$0{,}14 \pm 0{,}009$
p	$p \succ 0{,}05$				
SM_3	$2{,}14 \pm 0{,}11$	$2{,}18 \pm 0{,}12$	$2{,}16 \pm 0{,}17$	$2{,}19 \pm 0{,}15$	$2{,}08 \pm 0{,}12$
p	$p \succ 0{,}05$				
SM_4	$1{,}88 \pm 0{,}094$	$1{,}81 \pm 0{,}096$	$1{,}86 \pm 0{,}093$	$1{,}93 \pm 0{,}095$	$1{,}99 \pm 0{,}099$
p	$p \succ 0{,}05$				

4. DIFFERENTIAL DIAGNOSIS OF THE AGE OF THE FORMATION OF INJURIES TO INTERNAL ORGANS OF A PERSON BY MAPPING THE MAPS OF ELLIPTICITY OF POLARIZATION

The results of digital histology of histological sections of the liver of all groups by means of polarization mapping of ellipticity maps and statistical analysis of the temporal dynamics of changes in the average value, dispersion, skewness and kurtosis are presented in a series of fragments in Fig. 3 and table 3.

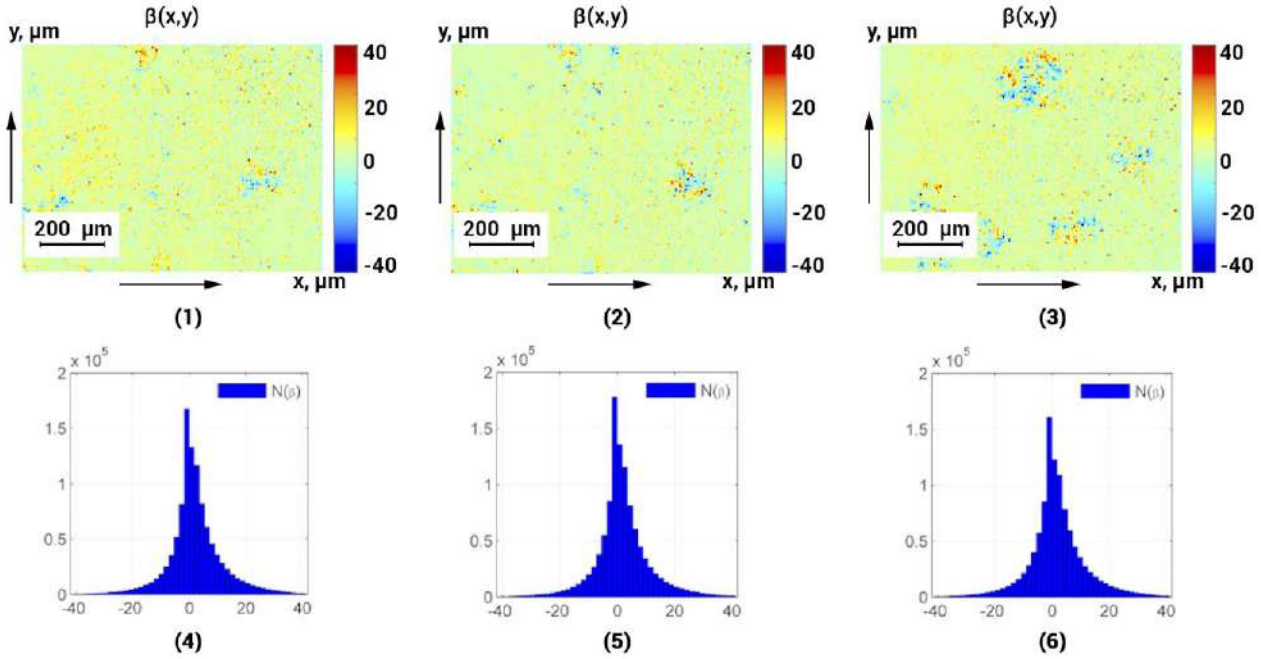

Fig. 3. Maps (fragments (1), (2), (3)) and histograms (fragments (4), (5), (6)) of the distributions of the polarization ellipticity of microscopic images (x4) of histological sections of the liver of deceased from the control group (fragments (1), (4)), research groups with different age of damage (6 hours - fragments (2), (5)) and (18 hours - fragments (3), (6)).

It was revealed that the polarization maps of ellipticity (Fig. 3, fragments (1) - (3) of small-scale (4x) microscopic images of samples of intact and damaged liver are topographically inhomogeneous (Fig. 4, fragments (4) - (6)).

Table 3 Time dynamics of changes in the statistical moments of the 1st - 4th orders, characterizing the distribution of the EP value of microscopic images (4x) of histological sections of the liver

T, hours	**2**	**4**	**6**	**12**	**18**
SM_1	$0{,}29 \pm 0{,}015$	$0{,}27 \pm 0{,}013$	$0{,}25 \pm 0{,}013$	$0{,}24 \pm 0{,}012$	$0{,}22 \pm 0{,}011$
p	$p \succ 0{,}05$				
SM_2	$0{,}22 \pm 0{,}011$	$0{,}205 \pm 0{,}09$	$0{,}19 \pm 0{,}009$	$0{,}18 \pm 0{,}009$	$0{,}17 \pm 0{,}008$
p	$p \succ 0{,}05$				
SM_3	$0{,}27 \pm 0{,}012$	$0{,}36 \pm 0{,}016$	$0{,}45 \pm 0{,}021$	$0{,}64 \pm 0{,}029$	$0{,}69 \pm 0{,}032$
p	$p \prec 0{,}05$				$p \succ 0{,}05$
SM_4	$0{,}41 \pm 0{,}019$	$0{,}52 \pm 0{,}21$	$0{,}63 \pm 0{,}031$	$0{,}88 \pm 0{,}037$	$0{,}92 \pm 0{,}049$
p	$p \prec 0{,}05$				$p \succ 0{,}05$
T, hours.	**24**	**30**	**36**	**42**	**48**
SM_1	$0.19 \pm 0{,}011$	$0{,}18 \pm 0{,}01$	$0{,}21 \pm 0{,}012$	$0{,}19 \pm 0{,}011$	$0{,}17 \pm 0{,}009$
p	$p \succ 0{,}05$				
SM_2	$0{,}18 \pm 0{,}009$	$0{,}16 \pm 0{,}008$	$0{,}14 \pm 0{,}008$	$0{,}15 \pm 0{,}009$	$0{,}17 \pm 0{,}009$
p	$p \succ 0{,}05$				
SM_3	$0{,}74 \pm 0{,}039$	$0{,}81 \pm 0{,}047$	$0{,}86 \pm 0{,}049$	$0{,}95 \pm 0{,}052$	$1{,}03 \pm 0{,}052$
p	$p \succ 0{,}05$				
SM_4	$1{,}02 \pm 0{,}055$	$1{,}08 \pm 0{,}056$	$1{,}14 \pm 0{,}063$	$1{,}23 \pm 0{,}72$	$1{,}17 \pm 0{,}071$
p	$p \succ 0{,}05$				

From the analysis of the data of statistical processing of the temporal changes in the coordinate distributions of the polarization ellipticity of microscopic images of liver samples with different age of damage (Table 3) follows the limited use of digital polarization histological examination - almost all changes in the value of statistical moments of the 1st - 4th orders are statistically unreliable ($p \succ 0{,}05$).

The exception is the asymmetry (dynamic range 0.37) and kurtosis (dynamic range 0.47) of the distributions of the polarization ellipticity, the values of which are linear and statistically significant, ($p \prec 0{,}05$) change in the time range with an age of up to 12 hours.

The results of digital histology using azimuthally invariant mapping of the polarization ellipticity of large-scale (40x) microscopic images of histological sections of the liver with different age of damage are shown in a series of fragments in Fig. 4.

Within the framework of the statistical approach to the analysis of azimuthally invariant digital histology data, the change in the tomographic structure of the ellipticity maps of liver samples with different age of damage is illustrated by the dynamics of changes in the magnitude of the statistical moments of the 1st - 4th orders, - Table 4.

Established:

- growth up to 18 hours of the diagnostic (linear) range of the temporal statistically significant ($p \prec 0{,}05$) change in the value of skewness(dynamic range 0.96) and kurtosis (dynamic range 1.04) of the distributions of the polarization ellipticity;

- the presence of a linear and statistically significant ($p \prec 0{,}05$) change in the dispersion of the distributions of the polarization ellipticity of large-scale microscopic images of histological sections of the liver at a time interval of up to 6 hours. (Dynamic range 0.05).

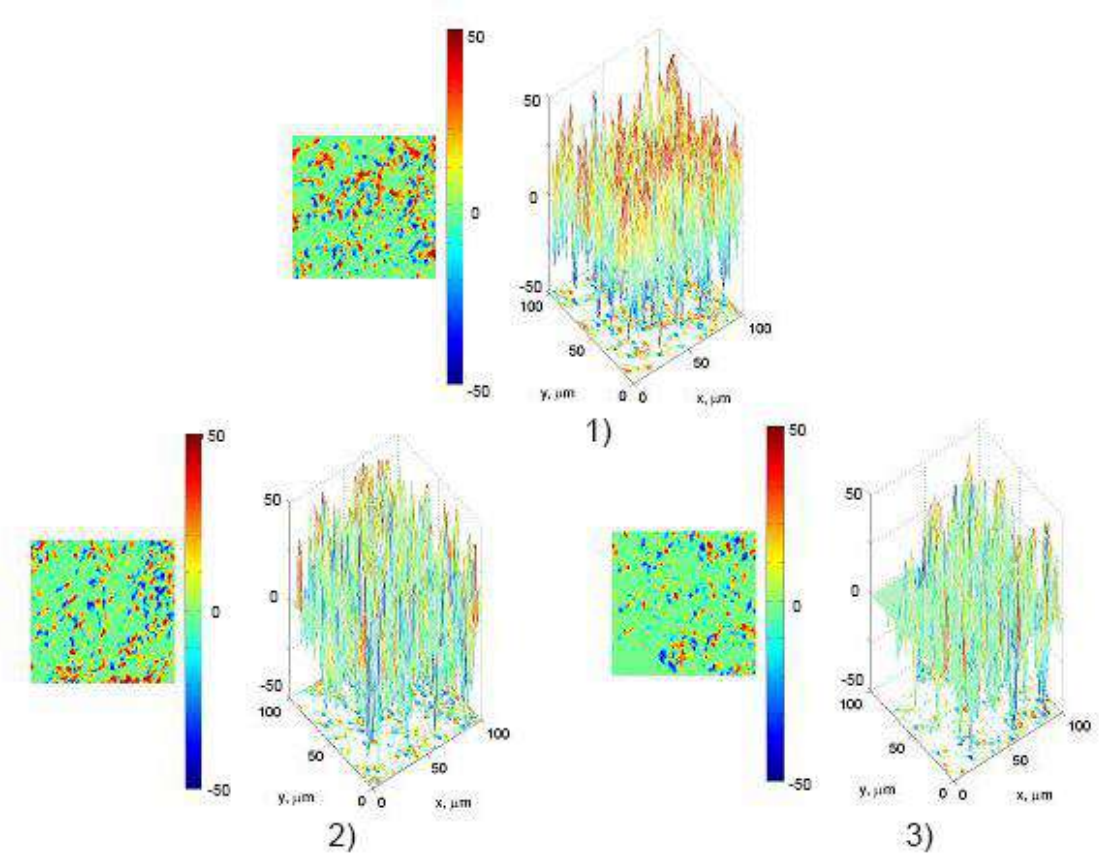

Fig. 4. Maps (fragments (1), (2), (3)) and distributions (fragments (4), (5), (6)) of the polarization ellipticity of microscopic images (x40) of histological sections of the liver of deceased from the control group (fragments (1) (4)), research groups with different duration of damage (6 hours - fragments (2), (5)) and (18 hours - fragments (3), (6))

Table 4 Time dynamics of changes in the statistical moments of the 1st - 4th orders, characterizing the distribution of EP

T, hours.	**2**	**4**	**6**	**12**	**18**
SM_1	$0{,}13 \pm 0{,}008$	$0{,}12 \pm 0{,}007$	$0{,}11 \pm 0{,}006$	$0{,}12 \pm 0{,}007$	$0{,}13 \pm 0{,}008$
p	$p \succ 0{,}05$				
SM_2	$0{,}11 \pm 0{,}006$	$0{,}105 \pm 0{,}005$	$0{,}09 \pm 0{,}005$	$0{,}08 \pm 0{,}005$	$0{,}105 \pm 0{,}006$
p		$p \prec 0{,}05$	$p \succ 0{,}05$		
SM_3	$0{,}61 \pm 0{,}028$	$0{,}79 \pm 0{,}036$	$0{,}97 \pm 0{,}041$	$1{,}34 \pm 0{,}069$	$1{,}57 \pm 0{,}072$
p	$p \prec 0{,}05$				
SM_4	$0{,}88 \pm 0{,}039$	$1{,}05 \pm 0{,}47$	$1{,}23 \pm 0{,}055$	$1{,}58 \pm 0{,}077$	$1{,}92 \pm 0{,}089$
p	$p \prec 0{,}05$				
T, hours	**24**	**30**	**36**	**42**	**48**

SM_1	$0.12 \pm 0{,}007$	$0{,}14 \pm 0{,}008$	$0{,}12 \pm 0{,}007$	$0{,}13 \pm 0{,}007$	$0{,}12 \pm 0{,}007$
p	$p \succ 0{,}05$				
SM_2	$0{,}09 \pm 0{,}005$	$0{,}11 \pm 0{,}006$	$0{,}13 \pm 0{,}007$	$0{,}11 \pm 0{,}006$	$0{,}09 \pm 0{,}005$
p	$p \succ 0{,}05$				
SM_3	$1{,}64 \pm 0{,}11$	$1{,}71 \pm 0{,}14$	$1{,}79 \pm 0{,}17$	$1{,}86 \pm 0{,}15$	$1{,}93 \pm 0{,}12$
p	$p \succ 0{,}05$				
SM_4	$2{,}02 \pm 0{,}14$	$2{,}06 \pm 0{,}16$	$1{,}91 \pm 0{,}23$	$1{,}99 \pm 0{,}25$	$2{,}11 \pm 0{,}21$
p	$p \succ 0{,}05$				

5. TIME INTERVALS AND ACCURACY OF THE POLARIZATION MAPPING METHOD

Table5 Time intervals and accuracy of the polarization mapping method for polarization azimuth maps

Brain				
Statistical moments	Interval, hours		Accuracy, min.	
Magnification	4x	40x	Magnification	4x
Average,	_	_	_	_
Dispersion,	_	_	_	_
Skewness,	12	18	60	55
Kurtosis,	12	18	60	55
Myocardium				
Statistical moments	Interval, hours		Accuracy, min.	
Magnification	4x	40x	4x	40x
Average,	_	_	_	_
Dispersion,	_	_	_	_
Skewness,	12	18	60	55
Kurtosis,	12	18	60	55
Liver				
Statistical moments	Interval, hours		Accuracy, min.	
Magnification	4x	40x	4x	40x
Average,	_	_	_	_
Dispersion,	_	_	_	_
Skewness,	12	18	70	60
Kurtosis,	12	18	70	60
Lung tissue				
Statistical moments	Interval, hours		Accuracy, min.	
Magnification	4x	40x	4x	40x
Average,	_	_	_	_
Dispersion,	_	_	_	_
Skewness,	12	18	70	60
Kurtosis,	12	18	70	60
Kidney				
Statistical moments	Interval, hours		Accuracy, min.	
Magnification	4x	40x	4x	40x
Average,	_	_	_	_
Dispersion,	_	_	_	_
Skewness,	12	18	65	60
Kurtosis,	12	18	65	60

Table 6 Time intervals and accuracy of the polarization mapping method for polarization ellipticity maps

Brain				
Statistical moments	Interval, hours		Accuracy, min.	
Magnification	4x	40x	4x	40x
Average,	_	_	_	_
Dispersion,	_	_	_	_
Skewness,	12	18	70	60
Kurtosis,	12	18	70	60
Myocardium				
Statistical moments	Interval, hours		Accuracy, min.	
Magnification	4x	40x	4x	40x
Average,	_	_	_	_
Dispersion,	_	_	_	_
Skewness,	12	18	70	60
Kurtosis,	12	18	70	60
Liver				
Statistical moments	Interval, hours		Accuracy, min.	
Magnification	4x	40x	4x	40x
Average,	_	_	_	_
Dispersion,	_	_	_	_
Skewness,	12	18	80	70
Kurtosis,	12	18	80	70
Lung tissue				
Statistical moments	Interval, hours		Accuracy, min.	
Magnification	4x	40x	4x	40x
Average,	_	_	_	_
Dispersion,	_	_	_	_
Skewness,	12	18	80	70
Kurtosis,	12	18	80	70
Kidney				
Statistical moments	Interval, hours		Accuracy, min.	
Magnification	4x	40x	4x	40x
Average,	_	_	_	_
Dispersion,	_	_	_	_
Skewness,	12	18	75	65
Kurtosis,	12	18	75	65

CONCLUSIONS

1. Azimuthally invariant polarization techniques of laser-induced digital histology of fluorophores in samples of human internal organs (brain, myocardium, lung tissue, liver, kidney) with different duration of damage - from 1 hour were experimentally tested up to 120 h.

2. Scenarios of changes in the statistical structure of maps of azimuth and ellipticity of polarization of microscopic images of histological sections of human internal organs have been determined - with an increase in the duration of damage, the value of the average and dispersion decreases, the skewness and kurtosis increase.

3. The following ranges of linear change in the variation in the magnitude of statistical indicators of polarization digital histology and the accuracy of determining the age of damage were revealed.:

3.1. Polarization azimuth maps of microscopic images with magnification 4x:

- skewness– 12 h.;

- kurtosis – 12 h.
- accuracy 60 min. – 70 min.

3.2. Polarization azimuth maps of microscopic images with magnification 40x:
- skewness – 12 h.;
- kurtosis – 12 h.
- accuracy – 55 min. – 60 min.

3.3. Polarization ellipticity maps of microscopic images with magnification 4x:
- skewness – 12 min.;
- kurtosis – 12 min.
- accuracy - 70 min. – 80 min.

3.4. Polarization ellipticity maps of microscopic images with magnification 40x:
- skewness – 12 h.;
- kurtosis – 12 h.
- accuracy – 65 h. – 75 h.

FUNDING

Current research supported by the National Research Foundation of Ukraine (Project 2020.02/0061)

REFERENCES

[1] V. Shankaran, J. T. Walsh, Jr., and D. J. Maitland, "Comparative study of polarized light propagation in biological tissues," J. Biomed. Opt. 7(3), 300–306 (2002).

[2] I. M. Stockford et al., "Analysis of the spatial distribution of polarized light backscattering," J. Biomed. Opt. 7(3), 313–320 (2002).

[3] X. Wang and L. V. Wang, "Propagation of polarized light in birefringent turbid media: a Monte Carlo study," J. Biomed. Opt. 7(3), 279–290 (2002).

[4] K. C. Hadley and I. A. Vitkin, "Optical rotation and linear and circular depolarization rates in diffusively scattered light from chiral, racemic, and achiral turbid media," J. Biomed. Opt. 7(3), 291–299 (2002).

[5] V. V. Tuchin, L. Wang, and D. A. Zimnyakov, Optical Polarization in Biomedical Applications, Springer, New York (2006).

[6] Angelsky, O.V., Bekshaev, A.Y., Hanson, S.G., Zenkova, C.Y., Mokhun, I.I., Jun, Z. Structured Light: Ideas and Concepts (2020) Frontiers in Physics, 8, 114.

[7] A. De Martino, Ed., "A polarization-based optical techniques applied to biology and medicine," in Proc. European Workshop, Ecole Polytechnique, Massy, France (2009).

[8] G. L. Coté and B. D. Cameron, "A noninvasive glucose sensor based on polarimetric measurements through the aqueous humor of the eye," in Handbook of Optical Sensing of Glucose in Biological Fluids and Tissues, V. V. Tuchin, Ed., pp. 183–211, CRC Press, Taylor & Francis Group, London (2009).

[9] Yu. A. Ushenko, V. P. Prysyazhnyuk, M. S. Gavrylyak, M. P. Gorsky, V. T. Bachinskiy, O. Ya. Vanchuliak, "Method of azimuthally stable Mueller-matrix diagnostics of blood plasma polycrystalline films in cancer diagnostics ," Proc. SPIE 9258, Advanced Topics in Optoelectronics, Microelectronics, and Nanotechnologies VII, 925807 (20 February 2015).

[10] Angelsky, O.V., Bekshaev, A.Y., Dragan, G.S., Maksimyak, P.P., Zenkova, C.Y., Zheng, J. Structured Light Control and Diagnostics Using Optical Crystals (2021) Frontiers in Physics, 9,715045.

[11] Angelsky, O.V., Maksimyak, P.P. Optical diagnostics of slightly rough surfaces (1992) Applied Optics, 31 (1), pp. 140-143.

[12] Angelsky, O.V., Zenkova, C.Y., Hanson, S.G., Zheng, J. Extraordinary Manifestation of Evanescent Wave in Biomedical Application (2020) Frontiers in Physics, 8, 159

[13] Ushenko, A.G., Burkovets, D.N., Ushenko, Yu.A. Polarization-Phase Mapping and Reconstruction of Biological Tissue Architectonics during Diagnosis of Pathological Lesions (2002) Optics and Spectroscopy (English translation of Optika i Spektroskopiya), 93 (3), pp. 449-456.

[14] Ushenko, A.G. Laser Polarimetry of Polarization-Phase Statistical Moments of the Object Field of Optically Anisotropic Scattering Layers (2001) Optics and Spectroscopy (English translation of Optika i Spektroskopiya), 91 (2), pp. 313-316.

[15] Angelsky, O.V., Ushenko, Y.A., Dubolazov, A.V., Telenha, O.Yu. The interconnection between the coordinate distribution of mueller-matrixes images characteristic values of biological liquid crystals net and the pathological changes of human tissues (2010) Advances in Optical Technologies, 130659.